IEEE Access
Multidisciplinary ⋮ Rapid Review ⋮ Open Access Journal

Received 29 June 2023, accepted 20 August 2023, date of publication 29 September 2023, date of current version 1 November 2023.

Digital Object Identifier 10.1109/ACCESS.2023.3320944

RESEARCH ARTICLE

Stability Bounds of Droop-Controlled Inverters in Power Grid Networks

PHILIPP C. BÖTTCHER[1,2], LEONARDO RYDIN GORJÃO[3], AND DIRK WITTHAUT[1,2,4]

[1]Institute of Energy and Climate Research–Systems Analysis and Technology Evaluation (IEK-STE), Forschungszentrum Jülich, 52428 Jülich, Germany
[2]Institute of Energy and Climate Research–Energy Systems Engineering (IEK-10), Forschungszentrum Jülich, 52428 Jülich, Germany
[3]Faculty of Science and Technology, Norwegian University of Life Sciences, 1432 Ås, Norway
[4]Institute for Theoretical Physics, University of Cologne, 50937 Köln, Germany

Corresponding author: Philipp C. Böttcher (p.boettcher@fz-juelich.de)

This work was supported in part by the Helmholtz Association via the Grant "Uncertainty Quantification—From Data to Reliable Knowledge (UQ)" under Grant ZT-I-0029, and in part by the Deutsche Forschungsgemeinschaft (DFG—German Research Foundation) under Grant 491111487.

ABSTRACT The energy mix of future power systems will include high shares of electricity generation by wind turbines and solar photovoltaics. These generation facilities are generally connected via power-electronic inverters. While conventional generation responds dynamically to the state of the electric power system, inverters are power-electronic hardware and need to be programmed to react to the state of the system. Choosing an appropriate control scheme and the corresponding parameters is necessary to guarantee that the system operates safely. A prominent control scheme for inverters is droop control, which mimics the response of conventional generation. In this work, we investigate the stability of coupled systems of droop-controlled inverters in arbitrary network topologies. Employing linear stability analysis, we derive effective local stability criteria that consider both the overall network topology as well as its interplay with the inverters' intrinsic parameters. First, we explore the stability of an inverter coupled to an infinite grid and uncover stability and instability regions. Second, we extend the analysis to a generic topology of inverters and provide mathematical criteria for the stability and instability of the system. Last, we showcase the usefulness of the criteria by examining two model systems using numerical simulations. The developed criteria show which parameters might lead to an unstable operating state.

INDEX TERMS Droop-controlled inverters, power-grid dynamics, linear stability analysis, small-signal stability.

I. INTRODUCTION

The ongoing transition to a sustainable energy system challenges the stability of electric power systems in several ways [1]. Renewable power sources, such as wind power and solar photovoltaics, fluctuate on a large range of time scales [2], [3], [4]. Wind power is often located at favorable locations far away from the centers of the load, requiring long-distance transmission [5]. Cellular or microgrid concepts are being developed to increase robustness, enabling small or islanded power systems to operate safely [6], [7]. Finally, wind turbines and solar panels are generally connected to the power grid via power-electronic inverters instead of traditional synchronous machines, which fundamentally alters frequency and voltage dynamics [8], [9]. A system driven by inverter-connected generation is fundamentally different from present systems around the world which still have a considerable amount of generation by large rotating generator masses. While conventional generation using large rotating masses is synchronously coupled to the grid due to electromechanical properties, inverters can be freely programmed to react to a measured state of the connected power grid. Different control algorithms have been proposed to achieve different targets. Studying how the dynamics of inverters are affected by different endogenous factors, e.g., different line types and model details [10], [11], becomes increasingly important as we move to a system dominated by power-electronic

The associate editor coordinating the review of this manuscript and approving it for publication was S. Sofana Reka.

inverters, particularly by droop-controlled inverters [12], [13], [14], [15]. Furthermore, it is essential to understand the collective dynamics of coupled inverters as well as how their interaction with the topology of the underlying power grid influences the set of system parameters that lead to a stable operating state. For example, the existence of different network motifs and topologies can destabilize the grid [16], induce multistability [17], [18], or influence the propagation of disturbances [19].

This article presents a set of analytically derived stability criteria for droop-controlled inverters. It extends upon previous studies on the topic, especially the ones by Schiffer et al., Refs. [20], [21], and [22] dealing with synchronous machines, by providing a discussion of the interplay of frequency, voltage dynamics, the power-grid topology, and their impact on the stability of the full system. Additionally, we make use of these criteria to derive a set of necessary and sufficient conditions for the linear stability of power grids with an arbitrary topology. In particular, we derive upper bounds for the reactive power droop gains and lower bounds for the connectivity of the network.

The paper is organized as follows. In Sec. II, we introduce the model used to describe the collective dynamics of inverter-based networks with the dynamics of droop-controlled inverters being described in Sec. II-A, the equations pertaining to the connecting power grid in Sec. II-B, and the stable states of operation or fixed points in Sec. II-C. In Sec. III, the dynamics of a single inverter coupled to an infinite grid are investigated to ascertain the existence of different regions of stability for different system parameters. Subsequently, we extend the stability analysis to arbitrary network topologies by constructing the Jacobian of the full system and formulating conditions for stability and instability in Sec. IV. In Sec. V, we extend these conditions to derive a set of explicit stability conditions expressed as inequalities. Finally, in Sec.VI, we test the tightness of the derived conditions and thus their usefulness in determining the stability of considered fixed points by numerical experiments in two test systems.

A list of reoccurring symbols and notations can be found in Table 1.

TABLE 1. List of reoccurring symbols and variables used in the subsequent chapters. Vectors are written as boldface lowercase Roman letters and matrices as boldface uppercase case Roman letters.

Symbol	Meaning
N	number of inverters
δ_j	power phase angle at inverter j
$\delta_{j,\ell}$	shorthand for $\delta_j - \delta_\ell$
E_j	voltage magnitude at inverter j
ω_j	angular frequency at inverter j
i	imaginary unit
$V_j = E_j e^{\mathrm{i}\delta_j}$	complex voltage at inverter j
I_j	complex current at inverter j
τ_j^V	recovery time of the voltage dynamics
τ_j	low-pass-filter time at inverter j
$P_j^{\mathrm{el}}, Q_j^{\mathrm{el}}$	active and reactive power at inverter j
S_j^{el}	apparent power $S_j^{\mathrm{el}}{=}P_j^{\mathrm{el}} + \mathrm{i}Q_j^{\mathrm{el}}$ at inverter j
$\cdot^d$	desired variable (e.g., desired frequency ω^d)
$P_j^{\mathrm{mes}}, Q_j^{\mathrm{mes}}$	measured active and reactive power at inverter j
κ_j, χ_j	droop gain for active and reactive power at inverter j
u_j, v_j	frequency and voltage control at inverter j
$\boldsymbol{Y} = \boldsymbol{G} + \mathrm{i}\boldsymbol{B}$	nodal admittance matrix
$\hat{y}_j = \hat{g}_j + \mathrm{i}\hat{b}_j$	shunt admittance at inverter j
$\cdot^\circ$	superscript for fixed point values of the state variables
ξ_j, ϵ_j, ν_j	small perturbation in power phase angle, voltage and frequency to the fixed point values at inverter j
$\cdot_s$	subscript indicating variables of the single inverter coupled to an infinite grid in Sec. III
$\hat{E}$	constant voltage of the infinite grid discussed in Sec. III
$\boldsymbol{J}$	Jacobian matrix describing the linearized dynamics around a fixed point
μ_n	nth eigenvalue of the Jacobian matrix $\boldsymbol{J}$
μ_{dom}	eigenvalue μ_i with the largest real part
$\boldsymbol{\Xi}$	reduced Jacobian matrix defined in Eq. (34)
$\boldsymbol{\Lambda}, \boldsymbol{A}, \boldsymbol{H}$	matrices derived in the linear stability analysis (see Eqs. (22) to (24))
$\boldsymbol{E}, \boldsymbol{T}, \boldsymbol{K}, \boldsymbol{X}$	diagonal matrices defined in Eqs. (25) to (28)
$\tilde{\boldsymbol{H}}$	abbreviation for $\boldsymbol{H} - \boldsymbol{X}^{-1}\boldsymbol{E}^{-1}$
λ_2	second smallest eigenvalue of the matrix $\boldsymbol{\Lambda}$
$\boldsymbol{v}_F$	Fielder vector of the corresponding eigenvalue λ_2
$\mathcal{D}_\perp^{(\cdot)}$	subspaces defined in Eq. (32)

II. MODELING INVERTER-BASED POWER GRIDS

A. DYNAMICS OF DROOP-CONTROLLED INVERTERS

Traditional power systems rely on synchronous machines to produce power and supply every consumer in the network with electricity. Synchronous machines possess an intrinsic relation between their power output and their frequency and phase angle, described by the swing equation [23]. Power-electronic inverters, on the contrary, do not possess such an intrinsic relation a priori but offer some flexibility to design their control mechanics and response. The vast majority of the commonly used inverters employ a control scheme that mimics the dynamics of conventional synchronous machines. In most cases, a simple proportional control is applied, whereas in fair argumentation the frequency regulation is designed to be an instantaneous reaction and the voltage control is regulated with a delay. These types of controllers are denoted droop controllers since they 'droop' or decrease their internal characteristics (frequency or voltage) to match a desired state of operation.

The basic state variables of a set of inverters $j = 1, \ldots, N$ are the voltage magnitude $E_j \in \mathbb{R}_+$ and the voltage power phase angle $\delta_j \in \mathbb{S}$. The control system adjusts these state values according to measurements of the active and reactive power exchanged with the grid. Following Schiffer et al. [21], a general control scheme for the inverter j obeys the equations

$$\begin{aligned} \dot{\delta}_j &= u_j, \\ \tau_j^V \dot{E}_j &= -E_j + v_j, \end{aligned} \tag{1}$$

where $\tau_j^V \in \mathbb{R}_+$ is the recovery time of the voltage dynamics under control. In a simple proportional, or droop, control scheme, the frequency control $u_j \in \mathbb{R}$ is directly proportional to the active power P_j^{el} and the voltage control $v_j \in \mathbb{R}$ is proportional to the reactive power Q_j^{el} (in VAR). Hence, the control signals read

$$\begin{aligned} u_j &= \omega^d - \kappa_j \left(P_j^{\mathrm{mes}} - P_j^d\right), \\ v_j &= E_j^d - \chi_j \left(Q_j^{\mathrm{mes}} - Q_j^d\right), \end{aligned} \tag{2}$$

and

$$\begin{aligned} \tau_j \dot{P}_j^{\mathrm{mes}} &= -P_j^{\mathrm{mes}} + P_j^{\mathrm{el}}, \\ \tau_j \dot{Q}_j^{\mathrm{mes}} &= -Q_j^{\mathrm{mes}} + Q_j^{\mathrm{el}}, \end{aligned} \tag{3}$$

where the superscript $\cdot^{\mathrm{mes}}$ indicates the measured values of active and reactive power and the superscript $\cdot^d$ stands for *desired*, i.e., referring to the desired frequency or voltage at inverter j. Naturally, the desired frequency ω^d the inverters should attain is unique across the power grid, whereas the desired voltage E_j^d depends on each inverter. A natural choice for the desired frequency is the reference frequency of 50 Hz or 60 Hz, i.e., the most common mains frequencies, which are within a certain range that balances the efficiency of generators and motors and certain requirements of equipment [23]. The parameters κ_j and χ_j are the droop gains for the active and reactive power, respectively.

The measurement of the active and reactive power is typically not instantaneous. This is taken into account by a low-pass filter such that the measured values P_j^{mes} and Q_j^{mes} at inverter j are given by Eq. (3) with a low-pass-filter time constant τ_j [24], where P_j^{el} and Q_j^{el} denote the instantaneous values.

We now summarize the equations of motion describing the inverter and its control system. The measured values of the power P_j^{mes} and Q_j^{mes} can be expressed in terms of the control signals using the relations Eq. (2). A further simplification can be made as the recovery time of the voltage dynamics is typically much lower than the time constant of the low-pass filter such that we can set $\tau_j^V = 0$ in Eq. (1), which yields $v_j = E_j$. Hence, we obtain the following set of equations of motion of an inverter j [20], [21]

$$\begin{aligned} \dot{\delta}_j &= \omega_j, \\ \tau_j \dot{\omega}_j &= -\omega_j + \omega^{\mathrm{d}} - \kappa_j \left(P_j^{\mathrm{el}} - P_j^{\mathrm{d}}\right), \\ \tau_j \dot{E}_j &= -E_j + E_j^{\mathrm{d}} - \chi_j \left(Q_j^{\mathrm{el}} - Q_j^{\mathrm{d}}\right). \end{aligned} \tag{4}$$

The active and reactive power exchanged with the grid, P_j^{el} and Q_j^{el}, depend on the state of all elements in the grid. To close the equations of motion we thus have to specify the network equations for the power grid.

B. THE NETWORK EQUATIONS

The active and reactive power flows in a power grid are described by the classical alternating current (AC) load-flow equations [23]. We consider a network consisting of inverter (active) and load (passive) nodes, which are modeled by a constant impedance to the ground. The passive nodes can be eliminated using the Kron reduction resulting in an effective network consisting of inverter nodes only [25]. In the following, we use this reduced network only. Without loss of generality, we can assume that the network is connected, as we can analyze different components separately otherwise.

The complex voltage at each inverter node $j = 1, \ldots, N$ is written as $V_j = E_j e^{\mathrm{i}\delta_j}$ with $E_j \in \mathbb{R}^+$ and $\delta_j \in \mathbb{S}$. The total current injected in the grid is linear in the voltages according to Ohm's law and can be written as

$$I_j = \sum_{\ell=1}^{N} Y_{j,\ell} V_\ell. \tag{5}$$

Here, we have introduced the nodal admittance matrix $\mathbf{Y} \in \mathbb{C}^{N\times N}$ with the entries

$$Y_{j,\ell} = G_{j,\ell} + \mathrm{i}B_{j,\ell} = \begin{cases} \hat{y}_j + \sum_{k\neq j} y_{j,k} & \text{if } j = \ell; \\ -y_{j,\ell} & \text{if } j \neq \ell, \end{cases} \tag{6}$$

where $y_{j,\ell}$ is the admittance between nodes j and ℓ in the effective Kron-reduced network. Furthermore, $\hat{y}_j = \hat{g}_j + \mathrm{i}\hat{b}_j$, where $\hat{g}_j$ and $\hat{b}_j$ denote the shunt conductance and susceptance, respectively. Without the shunts, the matrices $\boldsymbol{G}$ and $\boldsymbol{B}$ are graph Laplacian matrices [26].

The apparent power feed-in S_j^{el} at node j is given by

$$S_j^{\mathrm{el}} = V_j I_j^* = \sum_{\ell=1}^{N} V_j Y_{j,\ell}^* V_\ell^*, \tag{7}$$

where the superscript $*$ denotes the complex conjugate. Decomposing into active and reactive power, $S_j^{\mathrm{el}} = P_j^{\mathrm{el}} + \mathrm{i}Q_j^{\mathrm{el}}$, yields

$$P_j^{\mathrm{el}} = \sum_{\ell=1}^{N} E_j E_\ell \left[B_{j,\ell} \sin(\delta_{j,\ell}) + G_{j,\ell} \cos(\delta_{j,\ell})\right], \tag{8a}$$

$$Q_j^{\mathrm{el}} = \sum_{\ell=1}^{N} E_j E_\ell \left[-B_{j,\ell} \cos(\delta_{j,\ell}) + G_{j,\ell} \sin(\delta_{j,\ell})\right], \tag{8b}$$

using the shorthand $\delta_{j,\ell} = \delta_j - \delta_\ell$. In the main part of the manuscript, we restrict ourselves to lossless grids setting $G_{j,\ell}$ to zero. The network equations then read

$$P_j^{\mathrm{el}} = \sum_{\ell=1}^{N} E_j E_\ell B_{j,\ell} \sin(\delta_{j,\ell}), \tag{9a}$$

$$Q_j^{\mathrm{el}} = -\sum_{\ell=1}^{N} E_j E_\ell B_{j,\ell} \cos(\delta_{j,\ell}). \tag{9b}$$

For actual calculations, it is often convenient to use scaled units. In the per-unit (pu) system all voltages, currents, powers, and impedances are expressed in units of a suitably chosen reference value such that the load flow equations become dimensionless [23].

C. FIXED POINTS OF THE POWER GRID MODEL

The stationary operation of a power grid corresponds to a stable fixed point of the equations of motion Eq. (4). All voltages E_j, frequencies ω_j, and power phase angle differences $\delta_{j,\ell} = \delta_j - \delta_\ell$ must be constant in time to ensure a stationary power flow between the nodes of the grid. The condition of fixed phase differences requires that all machines rotate at the same frequency $\delta_j(t) = \bar{\omega}t + \delta_j^\circ$ for all $j = 1, \ldots, N$, leading to the conditions

$$\dot{\omega}_j = \dot{E}_j = 0, \quad \dot{\delta}_j = \bar{\omega}, \quad \text{for all } j = 1, \ldots, N. \tag{10}$$

In a mathematically strict sense, this defines a stable limit cycle of the system. However, all points of the cycle are physically equivalent and we can choose any point on the cycle as a representative of the equivalence class and call this an equilibrium. Perturbations along the limit cycle would simultaneously add or subtract a global phase shift δ from all phases δ_j, thus not affecting phase synchronization and power flows. These perturbations will be excluded from the stability analysis, which is expressed in Def. 1. In the following, we use the superscript $\cdot^\circ$ to denote the equilibrium values of phase angle, frequency, and voltage.

Using the equations of motion Eq. (4) and the network equations Eq. (9a) and Eq. (9b), the equilibria of an inverter-based power grid are described by the nonlinear algebraic equations

$$\begin{aligned}
\bar{\omega} &= \omega_j^\circ, \\
0 &= \omega^d - \omega_j^\circ + \kappa_j P_j^d - \kappa_j \sum_{\ell=1}^{N} B_{j,\ell} E_j^\circ E_\ell^\circ \sin(\delta_{j,\ell}^\circ), \\
0 &= E_j^d - E_j^\circ + \chi_j Q_j^d + \chi_j \sum_{\ell=1}^{N} B_{j,\ell} E_j^\circ E_\ell^\circ \cos(\delta_{j,\ell}^\circ).
\end{aligned} \tag{11}$$

Furthermore, we transform to a frame of reference that rotates with a constant angular velocity of $\bar{\omega}$. In this frame of reference, we have $\dot{\delta}_j = 0$ which simplifies the analysis. We note that several equilibria can coexist in networks with sufficiently complex topology, although such does not hinder performing linear stability analysis [27].

III. SINGLE INVERTER COUPLED TO AN INFINITE GRID

We first examine the simplest possible system, a single inverter coupled to an infinite grid. For this system, one can systematically compute all fixed points and scan over system parameters to obtain a comprehensive picture of the stability of the considered fixed point.

In this system, the voltage and frequency of the infinite grid are assumed to be constant at the reference level $\hat{E}$ and ω^d, respectively. In a rotating frame, we can further set the power phase angle of the grid to zero. Hence, we are left with the dynamics of the single inverter in terms of its voltage magnitude E_s, power phase angle δ_s, and frequency ω_s. The equations of motion Eq. (4) then read

$$\begin{aligned}
\dot{\delta}_s &= \omega_s, \\
\tau \dot{\omega}_s &= -\omega_s + \omega^d - \kappa(\hat{E} E_s B \sin(\delta_s) - P^d),
\end{aligned}$$

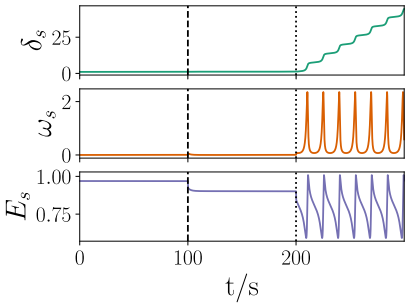

FIGURE 1. Simulation of a single inverter coupled to an infinite grid starting from a stable fixed point and increasing the reactive power droop gain χ. The remaining parameters where chosen as $\tau = 0.1$ s, $B = 1.5$, $\kappa = 1$, $P^d = 1.25$, $Q^d = 0.05$, $\hat{E} = 1$, and $E^d = 1$. Initially, the system is in a stable fixed point for a reactive power droop gain of $\chi_1 = 0.05$. After the reactive power droop gain is increased to $\chi_2 = 0.15$ at the dashed black line, the system moves to a new stable fixed point. Finally, the reactive power droop gain is increased to $\chi_3 = 0.3$ at the dotted black line. After the final change to χ_3, there is no stable fixed point and the dynamics exhibit a limit cycle behavior.

$$\begin{aligned}
\tau \dot{E}_s = &-E_s + E^d \\
&- \chi(-\hat{E} E_s B \cos(\delta_s) + B E_s^2 - Q^d).
\end{aligned} \tag{12}$$

where we have used that $B_{s,s} = -B_{s,\text{grid}} = -B$.

The fixed points of Eq. (12) can be written as $\boldsymbol{x}_s^\circ = (\delta_s^\circ, 0, E_s^\circ)^\top$, where the superscript $\top$ denotes the transpose of the vector. We can solve for the fixed points analytically by squaring the frequency and voltage equations to eliminate the fixed point power phase angle δ_s°. The fixed point voltages E_s° of Eq. (12) are thus determined by the equation

$$\begin{aligned}
0 = \; & B^2 E_s^{\circ 4} + 2\chi^{-1} B E_s^{\circ 3} \\
& + \left[\chi^{-2} - 2\kappa^{-1} B E^d - 2BQ^d - \hat{E}^2 B^2\right] E_s^{\circ 2} \\
& + \left[-2\chi^{-2}\left(E^d + \chi Q_d\right)\right] E_s^\circ \\
& + \left[E^d \chi^{-2} + 2\chi^{-1} Q^d E^d + Q^{d2} + \left(\frac{\omega^d}{\kappa}\right)^2 \right. \\
& \left. + 2\frac{\omega^d P^d}{\kappa} + P^{d2}\right],
\end{aligned} \tag{13}$$

which is a 4th-order polynomial in E_s° that can be solved analytically. Note that only real and positive solutions of Eq. (13) are physically meaningful and will be considered in the subsequent steps.

If a solution E_s° of Eq. (13) is found, the corresponding power phase angle δ_s° is given by

$$\delta_s^\circ = \arcsin\left(\frac{\omega_d/\kappa + P^d}{B\hat{E} E_s^\circ}\right). \tag{14}$$

Naturally, not every set of parameters guarantees a stable fixed point. Given a physically meaningful solution to Eq. (14), the argument of arcsine in Eq. (14) has to be in the interval $[-1, 1]$. Note, we also presupposed that the frequency ω_s° should vanish and thus we are only concerned with fixed points that meet this requirement. We now consider an example where we see how the stability of a fixed point may be lost such that the inverter becomes unstable. In the

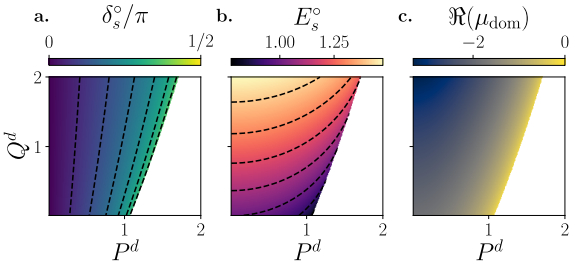

FIGURE 2. Scan over the desired reactive power Q^d and the desired active power P^d for a single inverter coupled to an infinite grid. The remaining parameters were chosen as $\tau = 0.1$ s, $B = 1.5$, $\kappa = 1$, $\chi = 0.5$, $\hat{E} = 1$, and $E^d = 1$. To classify how the fixed point changes for different parameters, the stationary power phase angle δ_s° (panel a), stationary voltage magnitude E_s° (panel b) and the dominant eigenvalue of the Jacobian μ_{dom} (panel c) are shown. The white color indicates regions where no stable fixed point could be found. The dashed lines show parameters on which the fixed point power phase angle or voltage magnitude take the same value.

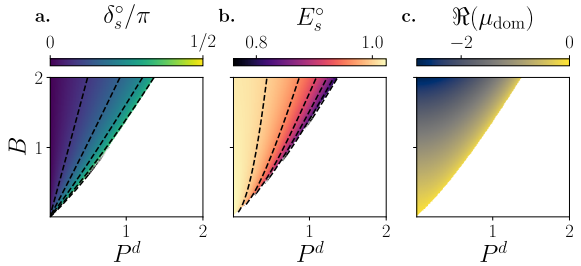

FIGURE 3. Scan over the coupling strength B and the desired active power P^d for a single inverter coupled to an infinite grid. The remaining parameters were chosen as $\tau = 0.1$ s, $Q_d = 0.05$, $\chi = 0.5$, $\kappa = 1$, $\hat{E} = 1$, and $E^d = 1$. To classify how the fixed point changes for different parameters, the stationary power phase angle δ_s° (panel a), stationary voltage magnitude E_s° (panel b) and the dominant eigenvalue of the Jacobian μ_{dom} (panel c) are shown. The white color indicates regions where no stable fixed point could be found. The dashed lines show parameters on which the fixed point power phase angle or voltage magnitude take the same value.

example shown in Fig. 1, the simulation was initialized in a fixed point calculated using Eq. (13) and Eq. (14). Subsequently, we increase the reactive power droop gain by starting with a reactive power droop gain $\chi_1 = 0.05$, increasing it to $\chi_2 = 0.15$ and to $\chi_3 = 0.3$ at the times indicated by the vertical black lines. The dynamics settles on a new fixed point after the first change to $\chi_2 = 0.15$ and the stability of the fixed point is lost after the change to $\chi_3 = 0.3$.

The local stability properties of an equilibrium, i.e., stability with respect to small perturbations, can be obtained by linearizing the equations of motion [28], [29]. We decompose the state variables into the values at the fixed point and small perturbations, which can be written as

$$\delta_s(t) = \delta_s^\circ + \xi_s(t),\ \omega_s(t) = \omega_s^\circ + \nu_s(t),\ E_s(t) = E_s^\circ + \epsilon_s(t). \tag{15}$$

We linearize Eq. (12) in the small perturbations around the fixed point $\boldsymbol{x}_s^\circ = (\delta_s^\circ, 0, E_s^\circ)^\top$. The linearized dynamics are given by

$$\frac{d}{dt}\begin{pmatrix}\xi_s\\ \nu_s\\ \epsilon_s\end{pmatrix} = \boldsymbol{J}_s \begin{pmatrix}\xi_s\\ \nu_s\\ \epsilon_s\end{pmatrix}, \tag{16}$$

where $\boldsymbol{J}_s \in \mathbb{R}^3$ is the Jacobian

$$\boldsymbol{J}_s = \begin{pmatrix} 0 & 1 & 0 \\ -\tau^{-1}\kappa E_s^\circ C & -\tau^{-1} & -\tau^{-1}\kappa S \\ -\tau^{-1}\chi E_s^\circ S & 0 & -\tau^{-1}\left[1+\chi\left(2BE_s^\circ - C\right)\right] \end{pmatrix}, \tag{17}$$

with $C = B\hat{E}\cos(\delta_s^\circ)$ and $S = B\hat{E}\sin(\delta_s^\circ)$.

The matrix $\boldsymbol{J}_s$ is the central object of linear stability analysis, with its eigenvalues and eigenvectors showing how a trajectory behaves close to a fixed point. The fixed point is asymptotically stable, i.e., the small disturbances $\xi_s(t)$, $\nu_s(t)$ and $\epsilon_s(t)$ decay exponentially, if all eigenvalues μ_n have a negative real part.

To understand which parameters lead to a stable fixed point, we scan over different parameter combinations. We focus on the desired active power P^d, the desired reactive power Q^d, the coupling strength B, and the reactive power droop gain χ. The active power P^d and reactive power Q^d are requirements of the connected consumers or producers of electricity, and B gives the coupling strength to the power grid network. The reactive power droop gain χ is a parameter that can be freely chosen by the grid operator. We choose $\hat{E} = 1$, $E^d = 1$, $\kappa = 1$ and $\tau = 0.1$ s if not stated otherwise. Note, while Q^d can in general be negative, we focus on the case of positive Q^d. In Fig. 2 we show the static power phase angle, static voltage, and the real part of the dominant eigenvalue examined over a range of values of P^d and Q^d, where $\chi = 0.5$ and $B = 1.5$ are fixed.

No stable fixed point can be found if the desired power P^d exceeds a critical threshold. The fixed point vanishes in a saddle-node bifurcation when the power phase angle takes the value $\delta_s^\circ = \pi/2$ and the real part of the dominant eigenvalue μ_{dom} is zero. Increasing the desired reactive power Q^d permits larger values for the desired active power P^d. Additionally, Fig. 2 also shows that the stationary power phase angle δ_s° is mostly influenced by the desired power P^d, while the stationary voltage E_s° is mostly influenced by the desired reactive power Q^d.

The scan over the coupling strength B and desired active power P^d can be seen in Fig. 3. The maximum P^d increases almost linearly with the coupling strength B for the chosen parameters. Again, the stationary power phase angle δ_s° assumes a maximum value close to the bifurcation.

The scan over different reactive power droop gains χ and desired power P^d (see Fig. 4) reveals that there is also a bifurcation for increasing the reactive power droop gain χ. In contrast to the parameters B, P^d and Q^d, the reactive power droop gain χ is a parameter that can be freely chosen in the inverters and is of large importance when trying to ensure the system stays in a stable state.

To highlight the influence of the reactive power droop gain χ in shaping the parameter region with a stable fixed point, the separatrices of different values of χ are shown in Fig. 5. For low values of χ, the separatrix in the

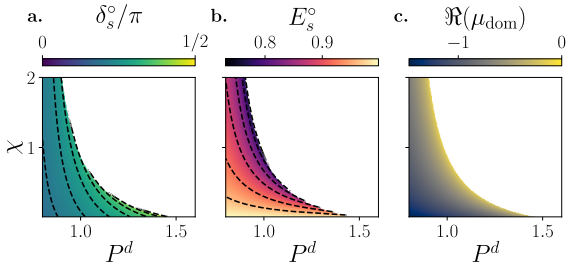

FIGURE 4. Scan over the reactive power droop gain χ and the desired active power P^d for a single inverter coupled to an infinite grid. The remaining parameters were chosen as $\tau = 0.1$ s, $Q_d = 0.05$, $B = 1.5$, $\kappa = 1$, $\hat{E} = 1$, and $E^d = 1$. To classify how the fixed point changes for different parameters, the stationary power phase angle δ_s° (panel a), stationary voltage magnitude E_s° (panel b) and the dominant eigenvalue of the Jacobian μ_{dom} (panel c) are shown. The white color indicates regions where no stable fixed point could be found. The dashed lines show parameters on which the fixed point power phase angle or voltage magnitude take the same value.

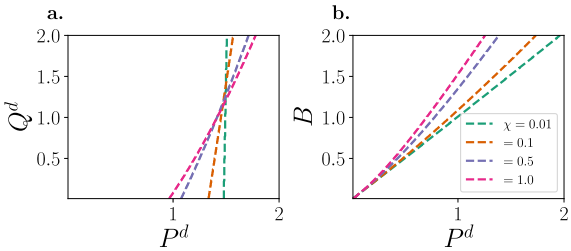

FIGURE 5. Shape of regions with stable fixed points of a single inverter coupled to an infinite grid for different values of the reactive power droop gain χ. Dashed lines show the border between parameter regions where a stable fixed point exists (left of the curves) and where no stable fixed point can be found (right of the curves). The coupling strength $B = 1.5$ and the desired reactive power $Q^d = 0.05$ were chosen for panel a and b, respectively. The remaining parameters were chosen as $\tau = 0.1$ s, $\kappa = 1$, $\hat{E} = 1$, and $E^d = 1$.

Q^d-P^d plane is almost vertical and P^d almost exclusively determines if a stable fixed point is present. This changes for increasing values of χ resulting in the separatrix describing approximately a linear function in the Q^d-P^d plane. Increasing the reactive power droop gain χ results in an overall smaller parameter region with a stable fixed point in the B-P^d plane. Thus, the network has to be reinforced, i.e., B has to be increased, to ensure that the fixed point is stable for the same P^d and increasing χ.

IV. LINEAR STABILITY ANALYSIS FOR EXTENDED NETWORKS

A. LINEAR STABILITY ANALYSIS

We now extend the linear stability analysis to systems consisting of multiple inverters that are coupled by an underlying network. As in the case of the single inverter, we linearize the equations of motion around the fixed point to find out if the perturbation $\xi_j(t)$, $\epsilon_j(t)$, and $\nu_j(t)$ decay exponentially, i.e., the fixed point is linearly stable. To this end, we decompose the state variables for each inverter j as the sum of their equilibrium values and the small perturbation as

$$\delta_j(t) = \delta_j^\circ + \xi_j(t),\ E_j(t) = E_j^\circ + \epsilon_j(t),\ \omega_j(t) = \omega_j^\circ + \nu_j(t). \tag{18}$$

Inserting this decomposition in the equations of motion Eq. (4) yields, at linear order

$$\dot{\xi}_j = \nu_j \tag{19}$$

$$\tau_j \dot{\nu}_j = -\nu_j - \kappa_j \sum_{\ell=1}^{N} \left(\Lambda_{j,\ell}\xi_\ell - A_{\ell,j}\epsilon_\ell\right), \tag{20}$$

$$\tau_j \dot{\epsilon}_j = -\epsilon_j + \chi_j E_j^\circ \sum_{\ell=1}^{N} \left(H_{j,\ell}\epsilon_\ell + A_{j,\ell}\xi_\ell\right), \tag{21}$$

where we have defined the matrices $\boldsymbol{\Lambda}, \boldsymbol{A}, \boldsymbol{H} \in \mathbb{R}^{N\times N}$ with components

$$\Lambda_{j,\ell} = \begin{cases} -E_j^\circ E_\ell^\circ B_{j,\ell}\cos(\delta_{\ell,j}^\circ) & \text{for} j \neq \ell, \\ \sum_{k\neq j} E_j^\circ E_k^\circ B_{j,k}\cos(\delta_{k,j}^\circ) & \text{for} j = \ell, \end{cases} \tag{22}$$

$$A_{j,\ell} = \begin{cases} -E_\ell^\circ B_{j,\ell}\sin(\delta_{\ell,j}^\circ) & \text{for} j \neq \ell, \\ \sum_k E_k^\circ B_{j,k}\sin(\delta_{k,j}^\circ) & \text{for} j = \ell, \end{cases} \tag{23}$$

$$H_{j,\ell} = \begin{cases} B_{j,\ell}\cos(\delta_{\ell,j}^\circ) & \text{for} j \neq \ell, \\ B_{j,j} + \sum_k B_{j,k}\cos(\delta_{k,j}^\circ)E_k^\circ/E_j^\circ & \text{for} j = \ell. \end{cases} \tag{24}$$

Furthermore, we define the diagonal matrices (all in $\mathbb{R}^{N\times N}$)

$$\boldsymbol{E} = \mathrm{diag}(E_1^\circ, E_2^\circ, \ldots, E_N^\circ), \tag{25}$$

$$\boldsymbol{T} = \mathrm{diag}(\tau_1, \tau_2, \ldots, \tau_N), \tag{26}$$

$$\boldsymbol{K} = \mathrm{diag}(\kappa_1, \kappa_2, \ldots, \kappa_N), \tag{27}$$

$$\boldsymbol{X} = \mathrm{diag}(\chi_1, \chi_2, \ldots, \chi_N). \tag{28}$$

In the following, we assume that all droop constants, i.e., κ and χ, and all time constants τ are strictly positive by design and we neglect the case that an equilibrium voltage vanishes exactly. Hence, the four matrices defined above all have strictly positive diagonal entries.

We can then summarize the linearized equations of motion in a vectorial form defining the vectors $\boldsymbol{\xi} = (\xi_1, \ldots, \xi_N)^\top$, $\boldsymbol{\nu} = (\nu_1, \ldots, \nu_N)^\top$, and $\boldsymbol{\epsilon} = (\epsilon_1, \ldots, \epsilon_N)^\top$, where the superscript $\top$ denotes the transpose of a matrix or vector. We obtain

$$\frac{d}{dt}\begin{pmatrix}\boldsymbol{\xi}\\ \boldsymbol{\nu}\\ \boldsymbol{\epsilon}\end{pmatrix} = \boldsymbol{J}\begin{pmatrix}\boldsymbol{\xi}\\ \boldsymbol{\nu}\\ \boldsymbol{\epsilon}\end{pmatrix}, \tag{29}$$

with the Jacobian matrix

$$\boldsymbol{J} = \begin{pmatrix}\mathbb{1} & \boldsymbol{0} & \boldsymbol{0}\\ \boldsymbol{0} & \boldsymbol{T}^{-1}\boldsymbol{K} & \boldsymbol{0}\\ \boldsymbol{0} & \boldsymbol{0} & \boldsymbol{T}^{-1}\boldsymbol{X}\boldsymbol{E}\end{pmatrix}\begin{pmatrix}\boldsymbol{0} & \mathbb{1} & \boldsymbol{0}\\ -\boldsymbol{\Lambda} & -\boldsymbol{K}^{-1} & \boldsymbol{A}^\top\\ \boldsymbol{A} & \boldsymbol{0} & \tilde{\boldsymbol{H}}\end{pmatrix}, \tag{30}$$

and the abbreviation $\tilde{\boldsymbol{H}} = \boldsymbol{H} - \boldsymbol{X}^{-1}\boldsymbol{E}^{-1}$.

Generally, an equilibrium is linearly (asymptotically) stable if the real part of all relevant eigenvalues of the Jacobian matrix $\boldsymbol{J}$ is strictly smaller than zero [28]. In this case, however, we must slightly adapt this definition. We note that $\boldsymbol{J}$ always has one eigenvalue $\mu_1 = 0$ with the eigenvector

$$(\boldsymbol{\xi}\ \boldsymbol{\nu}\ \boldsymbol{\epsilon})^\top = (\boldsymbol{1}\ \boldsymbol{0}\ \boldsymbol{0})^\top. \tag{31}$$

This eigenvector corresponds to a global shift of the inverters' phase angles $\boldsymbol{\delta} \mapsto \boldsymbol{\delta} + \alpha$ which has no physical significance

and must thus be excluded from the stability analysis. Hence, the linear stability analysis can be restricted to the subspaces

$$\mathcal{D}_{\perp}^{(3)} = \left\{(\boldsymbol{\xi}, \boldsymbol{\nu}, \boldsymbol{\epsilon}) \in \mathbb{R}^{3N} | (\mathbf{1}, \mathbf{0}, \mathbf{0})^{\top}(\boldsymbol{\xi}, \boldsymbol{\nu}, \boldsymbol{\epsilon}) = 0\right\}, \quad (32a)$$

$$\mathcal{D}_{\perp}^{(2)} = \left\{(\boldsymbol{\xi}, \boldsymbol{\epsilon}) \in \mathbb{R}^{2N} | (\mathbf{1}, \mathbf{0})^{\top}(\boldsymbol{\xi}, \boldsymbol{\epsilon}) = 0\right\}, \quad (32b)$$

$$\mathcal{D}_{\perp}^{(1)} = \left\{\boldsymbol{\xi} \in \mathbb{R}^{N} | \mathbf{1}^{\top}\boldsymbol{\xi} = 0\right\}. \quad (32c)$$

Furthermore, it is convenient to order the eigenvalues of the Jacobian as

$$\mu_1 = 0, \quad \Re(\mu_2) \leq \Re(\mu_3) \leq \cdots \leq \Re(\mu_{3N}). \quad (33)$$

We can now formulate a consistent condition for linear (asymptotic) stability transversally to the limit cycle (cf. Ref. [28]).

Definition 1: The equilibrium $(\delta_j^{\circ}, \omega_j^{\circ}, E_j^{\circ})$ *is linearly (asymptotically) stable if* $\Re(\mu_n) < 0$ *for all eigenvalues* $n = 2, \ldots, 3N$ *of the Jacobian matrix* $\boldsymbol{J}$ *defined in Eq. (30).*

B. THE REDUCED JACOBIAN

We can significantly simplify the linear stability analysis by eliminating the frequency subspace, leading to a reduced Jacobian of dimension $2N$ instead of $3N$. In particular, we obtain the following lemma

Lemma 1: The linear stability of an equilibrium $(\delta_j^{\circ}, \omega_j^{\circ}, E_j^{\circ})$ *is determined by the reduced Jacobian*

$$\boldsymbol{\Xi} = \begin{pmatrix} -\boldsymbol{\Lambda} & \boldsymbol{A}^{\top} \\ \boldsymbol{A} & \tilde{\boldsymbol{H}} \end{pmatrix}. \quad (34)$$

The equilibrium is stable if $\boldsymbol{\Xi}$ *is negative definite on* $\mathcal{D}_{\perp}^{(2)}$*. It is unstable if* $\boldsymbol{\Xi}$ *is not negative semi-definite on* $\mathcal{D}_{\perp}^{(2)}$*.*

Proof: Define the Lyapunov function candidate

$$V := \begin{pmatrix} \boldsymbol{\nu} \\ \boldsymbol{\xi} \\ \boldsymbol{\epsilon} \end{pmatrix}^{\top} \underbrace{\begin{pmatrix} \boldsymbol{K}^{-1}\boldsymbol{T} & 0 & 0 \\ 0 & \boldsymbol{\Lambda} & -\boldsymbol{A}^{\top} \\ 0 & -\boldsymbol{A} & -\tilde{\boldsymbol{H}} \end{pmatrix}}_{=:\boldsymbol{P}} \begin{pmatrix} \boldsymbol{\nu} \\ \boldsymbol{\xi} \\ \boldsymbol{\epsilon} \end{pmatrix}. \quad (35)$$

Then one finds

$$\begin{aligned} \dot{V} &= -2\boldsymbol{\nu}^{\top}\boldsymbol{K}^{-1}\boldsymbol{\nu} - 2(\boldsymbol{A}\boldsymbol{\xi} + \tilde{\boldsymbol{H}}\boldsymbol{\epsilon})^{\top}\boldsymbol{T}^{-1}\boldsymbol{X}\boldsymbol{E}(\boldsymbol{A}\boldsymbol{\xi} + \tilde{\boldsymbol{H}}\boldsymbol{\epsilon}) \\ &\leq 0. \end{aligned} \quad (36)$$

The last inequality follows as the matrices $\boldsymbol{T}, \boldsymbol{X}, \boldsymbol{K}$, and $\boldsymbol{E}$ are diagonal with only positive entries. If $\boldsymbol{\Xi}$ is negative definite, then $\boldsymbol{P}$ is positive definite and the equilibrium is stable according to the Lyapunov stability theorem. If $\boldsymbol{\Xi}$ is not negative semi-definite, then also $\boldsymbol{P}$ is not positive semi-definite and the equilibrium is unstable according to the Lyapunov instability theorem. □

V. EXPLICIT CONDITIONS FOR STABILITY AND INSTABILITY

In this section, we derive some explicit conditions for the stability or instability of an inverter-based grid. Guided by the results for the single inverter from Sec. III, we will focus on the role of the network connectivity and the reactive power droop gain χ. The starting point of our analysis is Lemma 1, for which we introduce a further decomposition into the voltage and angle subspace.

A. DECOMPOSING VOLTAGE AND ANGLE SUBSPACES

We can obtain further insight into the stability condition by a decomposition in terms of the rotor angle and the voltage dynamics. Applying the Schur or Albert complement [30] to the reduced Jacobian $\boldsymbol{\Xi}$, we obtain the following result.

Lemma 2 (Sufficient and Necessary Stability Conditions for Lossless Power Grids)

I. *The equilibrium* $(\delta_j^{\circ}, \omega_j^{\circ}, E_j^{\circ})$ *is linearly stable if (a) the matrix* $\boldsymbol{\Lambda}$ *is positive definite on* $\mathcal{D}_{\perp}^{(1)}$ *and (b) the matrix* $\tilde{\boldsymbol{H}} + \boldsymbol{A}\boldsymbol{\Lambda}^{+}\boldsymbol{A}^{\top}$ *is negative definite, where* $\cdot^{+}$ *is the Moore–Penrose pseudoinverse.*

II. *The equilibrium* $(\delta_j^{\circ}, \omega_j^{\circ}, E_j^{\circ})$ *is linearly stable if (a) the matrix* $\tilde{\boldsymbol{H}}$ *is negative definite and (b) the matrix* $\boldsymbol{\Lambda} + \boldsymbol{A}^{\top}\tilde{\boldsymbol{H}}^{-1}\boldsymbol{A}$ *is positive definite on* $\mathcal{D}_{\perp}^{(1)}$*.*

The equilibrium is linearly unstable if any of the above definiteness conditions are violated.

Proof: Here, we present solely the proof for criterion I, as an equivalent procedure can be used to prove criterion II. The reduced Jacobian matrix $\boldsymbol{\Xi}$ can be decomposed as

$$\boldsymbol{\Xi} = \boldsymbol{U}^{\top}\boldsymbol{S}\boldsymbol{U}, \quad (37)$$

with $\boldsymbol{S} \in \mathbb{R}^{2N \times 2N}$ a block diagonal matrix

$$\boldsymbol{S} = \begin{pmatrix} -\boldsymbol{\Lambda} & \mathbf{0} \\ \mathbf{0} & \tilde{\boldsymbol{H}} + \boldsymbol{A}\boldsymbol{\Lambda}^{+}\boldsymbol{A}^{\top} \end{pmatrix}, \quad (38)$$

and a transformation matrix

$$\boldsymbol{U} = \begin{pmatrix} \mathbb{1} & -\boldsymbol{\Lambda}^{+}\boldsymbol{A}^{\top} \\ 0 & \mathbb{1} \end{pmatrix}. \quad (39)$$

The transformation matrix $\boldsymbol{U}$ is of full rank and maps the vector $(\mathbf{1}, \mathbf{0})^{\top}$ onto itself. Hence, $\boldsymbol{U}$ also maps the relevant subspace $\mathcal{D}_{\perp}^{(2)}$ onto itself. Now assume that $\boldsymbol{S}$ is negative definite on $\mathcal{D}_{\perp}^{(2)}$. Then for every $\boldsymbol{x} \in \mathcal{D}_{\perp}^{(2)}, \boldsymbol{x} \neq \mathbf{0}$ we have

$$\boldsymbol{x}^{\top}\boldsymbol{\Xi}\boldsymbol{x} = (\boldsymbol{U}\boldsymbol{x})^{\top}\boldsymbol{S}(\boldsymbol{U}\boldsymbol{x}) < 0. \quad (40)$$

Similarly, if we assume that $\boldsymbol{\Xi}$ is negative definite on $\mathcal{D}_{\perp}^{(2)}$, then for every $\boldsymbol{y} \in \mathcal{D}_{\perp}^{(2)}, \boldsymbol{y} \neq \mathbf{0}$, we have

$$\boldsymbol{y}^{\top}\boldsymbol{S}\boldsymbol{y} = (\boldsymbol{U}^{-1}\boldsymbol{y})^{\top}\boldsymbol{\Xi}(\boldsymbol{U}^{-1}\boldsymbol{y}) < 0. \quad (41)$$

Hence, the transformation $\boldsymbol{U}$ does not affect the definiteness: $\boldsymbol{\Xi}$ is negative (semi-)definite on $\mathcal{D}_{\perp}^{(2)}$ if and only if $\boldsymbol{S}$ is negative (semi-)definite on $\mathcal{D}_{\perp}^{(2)}$.

Using Lemma 1 we know that the equilibrium is linearly stable if $\boldsymbol{\Xi}$ or equivalently $\boldsymbol{S}$ is negative definite on $\mathcal{D}_{\perp}^{(2)}$ and unstable if $\boldsymbol{\Xi}$ is not negative semi-definite. Since $\boldsymbol{S}$ is block diagonal, the definiteness of the entire matrix is equivalent to the definiteness of both blocks and the lemma follows. □

Lemma 2 allows us to obtain a deeper insight into the linear stability of inverter-based power grids and permits the

derivation of several explicit stability criteria. To this end, we will proceed through the conditions of the lemma step by step.

B. ANGLE STABILITY

Condition I. (a) in Lemma 2 refers to the stability of the isolated phase angle system, disregarding the voltage dynamics. To see this, we artificially fix the voltages such that $\epsilon = 0$. The linearized equations of motion read

$$\frac{\mathrm{d}}{\mathrm{d}t}\begin{pmatrix}\boldsymbol{\xi}\\ \boldsymbol{\nu}\end{pmatrix} = \begin{pmatrix}\mathbf{0} & \mathbb{1}\\ -\boldsymbol{T}^{-1}\boldsymbol{K}\boldsymbol{\Lambda} & -\boldsymbol{T}^{-1}\end{pmatrix}\begin{pmatrix}\boldsymbol{\xi}\\ \boldsymbol{\nu}\end{pmatrix}. \tag{42}$$

Performing the same simplification as in the previous sections, one finds that the system is stable if and only if the matrix $\boldsymbol{\Lambda}$ is positive definite on $\mathcal{D}_{\perp}^{(1)}$, which is identical to condition I.(a) in Lemma 2. One can now easily find a sufficient condition for angle stability. If for all connections (j, ℓ) in the grid we have

$$\cos(\delta_j^\circ - \delta_\ell^\circ) > 0, \tag{43}$$

then $\boldsymbol{\Lambda}$ is a proper Laplacian matrix of a weighted undirected network, which is well known to be positive definite on $\mathcal{D}_{\perp}^{(1)}$ [26].

Necessary and sufficient conditions are harder to obtain. If condition (43) is not satisfied for one or several connections, the matrix $\boldsymbol{\Lambda}$ rather describes a signed graph, for which positive definiteness is more involved. A variety of criteria have been obtained in [31], [32], [33], and [34].

In the following derivations, the Fiedler value or algebraic connectivity λ_2 and the corresponding Fiedler vector $\boldsymbol{\nu}_F$ will be used [35], [36], [37]. They are the smallest non-zero eigenvalue λ_2 of a Laplacian and the corresponding eigenvector $\boldsymbol{\nu}_F$. A Laplacian has at least one zero-valued eigenvalue $\lambda_1 = 0$. Further zero-valued eigenvalues correspond to the number of disjoint connected components in the network. The algebraic connectivity λ_2, as its name suggests, indicates how well-connected a network is. As the connection between different parts of the networks become weaker, λ_2 moves closer and closer to zero until the network separates into disjoint parts increasing the multiplicity of λ_1. Thus, the algebraic connectivity λ_2 encodes relevant information regarding the connectivity of the network and plays a crucial role in the stability analysis of networked systems.

C. VOLTAGE STABILITY

Condition II. (a) in Lemma 2 entails the stability of the isolated voltage subsystem. To see this, we artificially fix the angles such that $\boldsymbol{\nu} = \boldsymbol{\xi} = \mathbf{0}$. Then the linearized equations of motion read

$$\frac{\mathrm{d}}{\mathrm{d}t}\boldsymbol{\epsilon} = \boldsymbol{T}^{-1}\boldsymbol{X}\boldsymbol{E}\tilde{\boldsymbol{H}}\,\boldsymbol{\epsilon}. \tag{44}$$

Recall that the matrix $\boldsymbol{T}^{-1}\boldsymbol{X}\boldsymbol{E}$ is a diagonal matrix with strictly positive entries. Hence, we find that the isolated voltage dynamics is linearly stable if and only if the matrix $\tilde{\boldsymbol{H}}$ is negative definite, which is identical to condition II. (a) in Lemma 2.

We find a necessary and a sufficient condition for voltage stability in terms of the droop constants (cf. [38]). Both show that the droop gains for the reactive power χ must not be chosen too large.

Corollary 1: If for all nodes $j = 1, \ldots, N$,

$$\frac{1}{\chi_j} > \sum_{\ell=1}^{N} B_{j,\ell}(E_j^\circ + E_\ell^\circ) \tag{45}$$

and condition (43) holds for all connections (j, ℓ) in a power grid, then the matrix $\tilde{\boldsymbol{H}}$ is negative definite and the voltage subsystem is stable.

Proof: By applying Geršgorin's circle theorem [39] to the matrix $\tilde{\boldsymbol{H}}$, the following condition for its eigenvalues α_j, $\forall j$ stands

$$|\alpha_j - \mathcal{C}_j| \leq R_j, \tag{46}$$

where

$$\begin{aligned}\mathcal{C}_j &= \tilde{H}_{j,j} = H_{j,j} - (\boldsymbol{E}^{-1}\boldsymbol{X}^{-1})_{j,j}\\ &= B_{j,j} + \sum_k B_{j,k}\cos(\delta_k^\circ - \delta_j^\circ)\frac{E_k^\circ}{E_j^\circ} - \frac{1}{\chi_j E_j^\circ}\\ R_j &= \sum_{\ell\neq j}^{N} |B_{j,\ell}\cos(\delta_j^\circ - \delta_l^\circ)|,\end{aligned} \tag{47}$$

are the center and the radius of the Geršgorin disk, respectively. All eigenvalues are guaranteed to lie in the left half of the complex plane, which yields the negative definiteness, if $\mathcal{C}_j + R_j < 0$ for all $j = 1, \ldots, N$. Evaluating this condition yields

$$\begin{aligned}\frac{1}{\chi_j} > \; & B_{j,j}E_j^\circ + \sum_k B_{j,k}\cos(\delta_k^\circ - \delta_j^\circ)E_k^\circ\\ & + \sum_{\ell\neq j}^{N} E_j^\circ |B_{j,\ell}\cos(\delta_j^\circ - \delta_\ell^\circ)|.\end{aligned} \tag{48}$$

Using the bound $\cos(\cdot) \leq 1$, $|\cos(\cdot)| \leq 1$, and the positivity of $B_{j,\ell}$, a sufficient condition for negative definiteness of $\tilde{\boldsymbol{H}}$ is obtained as

$$\frac{1}{\chi_j} > \sum_{\ell=1}^{N} B_{j,\ell}(E_j^\circ + E_\ell^\circ). \tag{49}$$

This concludes the proof. □

Corollary 2: If for any subset of nodes $\mathcal{S} \subseteq \{1, 2, \ldots, N\}$,

$$\sum_{j\in\mathcal{S}} \frac{1}{\chi_j E_j^\circ} \leq \sum_{j,\ell\in\mathcal{S}} H_{j,\ell}, \tag{50}$$

then the matrix $\tilde{\boldsymbol{H}}$ is not negative definite and the equilibrium is linearly unstable.

Proof: This result follows from evaluating the expression $\boldsymbol{x}^\top\tilde{\boldsymbol{H}}\boldsymbol{x}$ for a trial vector $\boldsymbol{x} \in \mathbb{R}^N$ with entries $x_j = 1$ $\forall j \in \mathcal{S}$ and $x_j = 0$ $\forall j \notin \mathcal{S}$. □

D. COUPLED STABILITY CRITERIA

We have shown that part (a) of both stability criteria in Lemma 2 refer to each isolated subsystem. Hence both must be stable in themselves to enable linear stability of the full dynamical system. The remaining parts (b) of the stability criteria then refer to the coupled frequency and voltage dynamics. These criteria are significantly stricter than the isolated criteria. To see this, we focus on criterion I in Lemma 2, assuming that $\boldsymbol{\Lambda}$ is positive definite on $\mathcal{D}_{\perp}^{(1)}$. The complementary condition I. (b) is

$$\tilde{\boldsymbol{H}} + \boldsymbol{A}\boldsymbol{\Lambda}^{+}\boldsymbol{A}^{\top} \prec 0, \tag{51}$$

where $\boldsymbol{Z} \prec 0$ is used as a short hand for $\boldsymbol{Z}$ being negative definite. This condition is stricter than the condition of pure voltage stability, $\tilde{\boldsymbol{H}} \prec 0$. Hence, the stability of the two isolated subsystems is not sufficient. Instead, they must comprise a certain 'security margin' quantified by the second term on the left-hand side of Eq. (51) in order to maintain linear stability.

We now present several explicit stability criteria, focusing on the interplay of internal dynamics and the grid topology. We typically assume that the two isolated subsystems are stable, i.e., conditions I. (a) and II. (a) in Lemma 2 are satisfied unless stated otherwise. First, we consider the case of small reactive power droop gains, as this is necessary to ensure voltage stability, see Corollaries 1 and 2, and relate stability to the connectivity of the grid.

Corollary 3: A necessary condition for the stability of an equilibrium point is given by

$$\lambda_2 > \sum_{j=1}^{N} \chi_j E_j^{\circ} \left[\sum_{k=1}^{N} A_{j,k} v_{Fk} \right]^2 + \mathcal{O}(\chi_j^2), \tag{52}$$

where λ_2 is the network's algebraic connectivity and $\boldsymbol{v}_F$ denotes the Fiedler vector of the Laplacian $\boldsymbol{\Lambda}$ for $\chi_j \equiv 0$.

Proof: A normalized Fiedler vector $\boldsymbol{v}_F$ is defined at $\chi_j \equiv 0$ [35], [36], [37]. The actual normalized Fiedler vector, for a particular non-zero value of the χ_j, is denoted $\boldsymbol{v}_F'$, such that

$$\boldsymbol{v}_F' = \boldsymbol{v}_F + \mathcal{O}(\chi_j). \tag{53}$$

Following criterion II. (b) in Lemma 2, the stability of the fixed point requires that all vectors $\boldsymbol{y}$ obey

$$\boldsymbol{y}^{\top}\boldsymbol{\Lambda}\boldsymbol{y} > -\boldsymbol{y}^{\top}\boldsymbol{A}^{\top}\tilde{\boldsymbol{H}}^{-1}\boldsymbol{A}\boldsymbol{y}. \tag{54}$$

Now we consider the particular choice $\boldsymbol{y} = \boldsymbol{v}_F'$ to obtain a necessary condition for stability. The left-hand side of condition (54) then simplifies to $\boldsymbol{v}_F'^{\top}\boldsymbol{\Lambda}\boldsymbol{v}_F' = \lambda_2$. To simplify the right-hand side, we expand the matrix inverse according to

$$\begin{aligned} -\tilde{\boldsymbol{H}}^{-1} &= (\boldsymbol{E}^{-1}\boldsymbol{X}^{-1} - \boldsymbol{H})^{-1} = \sum_{\ell=0}^{\infty} \boldsymbol{E}\boldsymbol{X}(\boldsymbol{E}\boldsymbol{X}\boldsymbol{H})^{\ell}, \\ &= \boldsymbol{E}\boldsymbol{X} + \mathcal{O}(\chi_j^2). \end{aligned} \tag{55}$$

Substituting this expansion into condition (54), we obtain the necessary condition to leading order in the reactive power droop gains,

$$\lambda_2 > \boldsymbol{v}_F^{\top}\boldsymbol{A}^{\top}\boldsymbol{E}\boldsymbol{X}\boldsymbol{A}\boldsymbol{v}_F + \mathcal{O}(\chi_j^2). \tag{56}$$

An equivalent result in synchronous generators can be found in Ref. [38] and this concludes the proof. □

We recall that a necessary and sufficient criterion for the stability of the isolated frequency subsystem is given by $\lambda_2 > 0$. In contrast, the right-hand side of condition (52) is generally positive. Hence, additional algebraic connectivity is needed in the grid as a 'security margin' to guarantee the stability of the whole dynamical system.

We can further derive two sufficient stability criteria, one in terms of the reactive power droop gains χ by extending Corollary 1 and one in terms of the algebraic connectivity λ_2 of the network.

Corollary 4: An equilibrium is linearly stable if the network's algebraic connectivity is positive, $\lambda_2 > 0$, and the reactive power droop gains satisfy

$$\frac{1}{\chi_j} > \sum_{\ell=1}^{N} B_{j,\ell} + E_j^{\circ} \frac{\|\boldsymbol{A}\|_2 \|\boldsymbol{A}^{\top}\|_2}{\lambda_2}, \tag{57}$$

for all nodes $j = 1, \ldots, N$, where $\|\cdot\|_2$ is the induced ℓ_2-norm.

Proof: A positive algebraic connectivity $\lambda_2 > 0$ implies that both $\boldsymbol{\Lambda}$ is positive definite on $\mathcal{D}_{\perp}^{(1)}$ and criterion I. (a) in Lemma 2 is satisfied.

Consider now criterion I. (b). Using the same arguments as in the proof of Corollary 1 one can show that the conditions Eq. (57) imply that the matrix

$$\tilde{\boldsymbol{H}} + \frac{\|\boldsymbol{A}\|_2 \|\boldsymbol{A}^{\top}\|_2}{\lambda_2} \mathbb{1} \tag{58}$$

is negative definite. Noting that $\lambda_2^{-1} = \|\boldsymbol{\Lambda}^{+}\|_2$ and using the sub-multiplicativity of the ℓ_2-norm, we then find that $\forall \boldsymbol{y} \neq \boldsymbol{0}$ we have

$$\begin{aligned} & \boldsymbol{y}^{\top}\left[-\tilde{\boldsymbol{H}} - \frac{\|\boldsymbol{A}\|_2 \|\boldsymbol{A}^{\top}\|_2}{\lambda_2}\right]\boldsymbol{y} > 0 \\ \Leftrightarrow\ & \boldsymbol{y}^{\top}\left[\boldsymbol{E}^{-1}\boldsymbol{X}^{-1} - \boldsymbol{H}\right]\boldsymbol{y} > \|\boldsymbol{A}\|_2 \|\boldsymbol{\Lambda}^{+}\|_2 \|\boldsymbol{A}^{\top}\|_2 \|\boldsymbol{y}\|^2 \\ & \qquad \geq \|\boldsymbol{A}\boldsymbol{\Lambda}^{+}\boldsymbol{A}^{\top}\|_2 \|\boldsymbol{y}\|^2 \\ & \qquad \geq \boldsymbol{y}^{\top}\boldsymbol{A}\boldsymbol{\Lambda}^{+}\boldsymbol{A}^{\top}\boldsymbol{y} \\ \Leftrightarrow\ & \boldsymbol{y}^{\top}\left[\boldsymbol{E}^{-1}\boldsymbol{X}^{-1} - \boldsymbol{H} - \boldsymbol{A}\boldsymbol{\Lambda}^{+}\boldsymbol{A}^{\top}\right]\boldsymbol{y} > 0. \end{aligned} \tag{59}$$

Hence, matrix $\tilde{\boldsymbol{H}} + \boldsymbol{A}\boldsymbol{\Lambda}^{+}\boldsymbol{A}^{\top}$ is negative definite. Criterion I. (b) in Lemma 2 is satisfied and the equilibrium is linearly stable. □

The condition given by Corollary 4 highlights that a stable fixed point needs both a sufficiently large algebraic connectivity λ_2 and low reactive power droop gains χ.

Corollary 5: If by criterion II. (a) in Lemma 2 the matrix $\tilde{\boldsymbol{H}}$ is negative definite, and if the algebraic connectivity λ_2 satisfies

$$\lambda_2 > \|\boldsymbol{A}^{\top}\tilde{\boldsymbol{H}}^{-1}\boldsymbol{A}\|_2, \tag{60}$$

where $\|\cdot\|_2$ is the induced ℓ_2-norm, then the equilibrium point is linearly stable.

Proof: Condition II. (a) in Lemma 2 is satisfied by assumption, so we can focus on condition II. (b)

The assumption (60) implies that $\forall \boldsymbol{y} \in \mathcal{D}_{\perp}^{(1)}$

$$\begin{aligned} \boldsymbol{y}^{\top}\boldsymbol{\Lambda}\boldsymbol{y} &\geq \lambda_2 \|\boldsymbol{y}\|^2 \\ &> \|\boldsymbol{A}^{\top}\tilde{\boldsymbol{H}}^{-1}\boldsymbol{A}\|_2 \|\boldsymbol{y}\|^2 \\ &\geq \boldsymbol{y}^{\top}\boldsymbol{A}^{\top}\tilde{\boldsymbol{H}}^{-1}\boldsymbol{A}\boldsymbol{y}, \end{aligned} \tag{61}$$

such that the matrix $\boldsymbol{\Lambda}+\boldsymbol{A}^{\top}\tilde{\boldsymbol{H}}^{-1}\boldsymbol{A}$ is positive definite on $\mathcal{D}_{\perp}^{(1)}$. Condition II. (b) in Lemma 2 is therefore satisfied and the equilibrium is linearly stable. □

VI. TESTING THE USEFULNESS OF THE STABILITY CRITERIA

We now compare the findings above to numerical results for two test systems. One system consists of two inverters and the other consists of ten inverters arranged in a tree-like topology. In both cases, a subset of the inverters act as net producers of electricity, which can be seen as inverters injecting power into the system, e.g., solar panels or wind turbines, and the remaining inverters act as consumers, which could, for example, be batteries that are being charged for later consumption. One of the inverters serves as a slack node. At this inverter, the phase is set to $\delta_{\text{slack}} = 0$, the voltage magnitude is kept at $E_{\text{slack}} = 1$, and the equations for the active and reactive power are not considered. The slack node acts as an ideal voltage source that can provide an arbitrary amount of power. Hence, we exclude the conditions in Eq. (11) for the slack node when calculating the fixed point. If needed, the active and reactive power injections at the slack node can be computed afterward.

As in the example for the single inverter discussed in Sec. III, the desired frequency is set to $\omega^d = 0$. Since we are in a co-rotating reference frame, this corresponds to synchronized dynamics with the reference frequency. The desired voltage was set to $E^d = 1$, the low-pass-filter time to $\tau = 0.1\,\text{s}$, the active power droop gain $\kappa = 1$, and the desired reactive power to $Q^d = 0.05$. In both cases, we will examine a scan over different values of desired power P^d, coupling strength B, and reactive power droop gains χ.

The two-inverter system has one inverter with a desired active power of $P_1^d = P^d$ and one with $P_2^d = -P^d$. Tracking the physical fixed points, determining their stability, and evaluating Corollaries 4 and 5 leads to the stability maps that can be seen in Fig. 6. For a given desired power P^d, a stable fixed point only exists if the coupling strength B is sufficiently high and the reactive power droop gain χ is kept relatively constrained. The critical value of the coupling strength B increases super-linearly with the desired power P^d, while the critical reactive power droop gain decreases with P^d.

We generally find a good agreement between the explicit stability criteria and the stability boundary resulting from the evaluation of the eigenvalues of the Jacobian. In particular, Corollaries 4 and 5, which represent sufficient conditions for stability, capture the general shape of the separatrix between stability and instability. Notably, there is a small region where

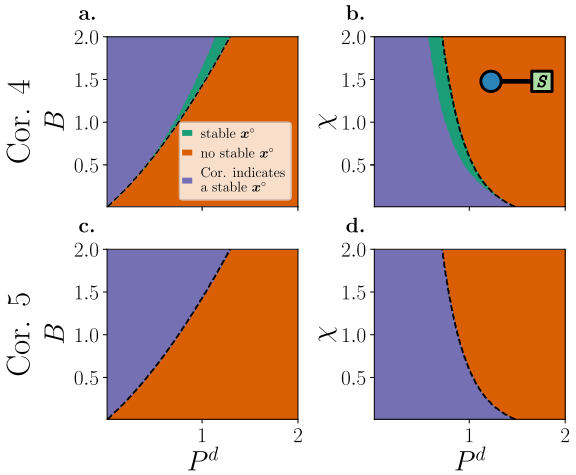

FIGURE 6. Corollary 4 (top row) and Corollary 5 (bottom row), sufficient conditions for stability, result in a tight bound for the region with a stable fixed point for a two-inverter system. A schematic representation of the network is shown in the inset in the upper right of panel b, with one of the inverters acting as a slack node (indicated by *S*). Panels a and c are the results of a scan over P^d and the coupling strength B, and panels b and d are the results of a scan over P^d and the reactive power droop gain χ. The reactive power droop gain was chosen as $\chi = 0.5$ for the scan in the B-P^d plane in panels a and c, and the coupling strength $B = 1.5$ was chosen for the scan in the χ-P^d plane in panels b and d. Additionally, the low-pass-filter time $\tau = 0.1$ s, the active power droop gain $\kappa = 1$, desired voltage $E^d = 1$, and desired reactive power $Q^d = 0.05$ were chosen. The different colors show where the fixed point is stable or unstable, and where the corollaries indicate a stable fixed point. The separatrix between stable and no-stable fixed points regions is given by the dashed black line. Note that the region where the Corollaries 4 and 5 imply the stability of the fixed point always overlays the region where the full Jacobian indicates a stable fixed point.

the fixed point is stable, while Corollary 4 does not point to a stable fixed point. This is to be expected as Corollary 4 is merely a sufficient condition.

Subsequently, we investigate a system with $N = 10$ nodes in a tree-like power grid (see inset in panel **b** in Fig. 7) The outer nodes are net producers of power (e.g., solar panels) providing power to the four inner nodes that are net consumers of power. While the outer nodes have a desired active power of $P^{d,f}$, the inner ones have a desired active power of $-3P^{d,f}/2$. In this case, the central node acts as the slack node. The overall shape of the parameter region with a stable fixed point (see Fig. 7) is similar to the previously treated cases. A minimum value of the coupling strength B is required for a stable fixed point, where the critical value increases super-linearly with $P^{d,f}$ (see panel **a**.). Furthermore, the reactive power droop gains χ must not exceed a critical value, which decreases with increasing $P^{d,f}$ (see panel **b**.). In general, Corollaries 4 and 5 describe the shape of the stable parameter region well. Note, in comparison with the two-inverter system (see Fig. 6), the region where Corollaries 4 and 5 indicate a stable fixed point is smaller. This highlights again that Corollaries 4 and 5 are sufficient conditions for a stable fixed point that conservatively predict the stable parameter region.

In summary, the numerical simulations of the two considered test systems show the usefulness of the developed corollaries. The developed corollaries highlight the role of

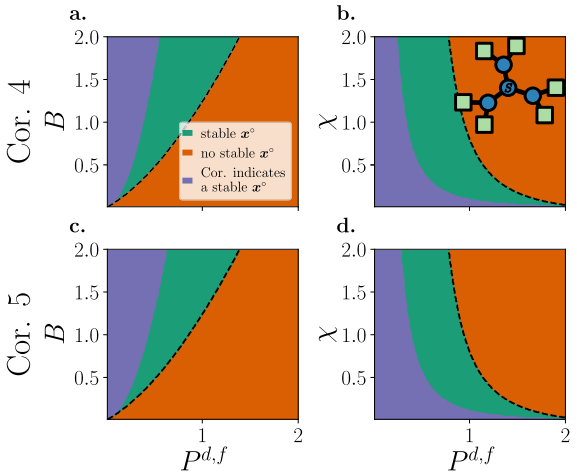

FIGURE 7. Corollary 4 (top row) and Corollary 5 (bottom row), sufficient conditions for stability, correctly identify the region with stable fixed points for a considerable region in parameter space for a tree-like topology. The six outer nodes deliver power, while the inner four ones consume power (see inset in panel b). A slack node with fixed voltage magnitude $E_1 = 1$ and the reference power phase angle $\delta_1 = 0$ is located at the center (indicated by S). The reactive power droop gain was chosen as $\chi = 0.5$ for the scan in the B-$P^{d,f}$ plane in panel a and c, and the coupling strength $B = 1.5$ was chosen for the scan in the χ-$P^{d,f}$ plane in panel b and d. Additionally, the low-pass-filter time $\tau = 0.1$ s, the active power droop gain $\kappa = 1$, desired voltage $E^d = 1$, and desired reactive power $Q^d = 0.05$ were chosen. The different colors show where the fixed point is stable or unstable, and where the corollaries indicate a stable fixed point. The separatrix between stable and no-stable fixed points regions is given by the dashed black line. Note that the region where the Corollaries 4 and 5 imply the stability of the fixed point always overlays the region where the full Jacobian indicates a stable fixed point.

different parameters, in particular, the reactive power droop gains χ, in shaping the parameter region with a stable fixed point. As the corollaries were developed analytically, they reveal the interplay of these parameters in a general and transparent way.

VII. CONCLUSION AND DISCUSSION

In this article, we investigated the collective dynamics of a network of droop-controlled inverters. Modern power grids rely evermore on power-electronic devices given the increased penetration of renewable energy sources. Since droop-controlled inverters are a promising type of power-electronic inverters, we need to understand how systems of connected droop-controlled inverters behave dynamically. More specifically, we need to know the combination of values for the intrinsic parameters of each inverter that ensure the desired operating state, i.e., the fixed point, is stable. We started by considering a single inverter coupled to an infinite grid. Using this simple setting, all fixed points and their stability could be determined analytically. Scanning over the desired active power P^d, the reactive power Q^d, the coupling strength to the power grid B, and the reactive power droop gain χ reveals when the single inverter can operate at a stable fixed point. The numerical results show that the existence of a stable fixed point necessitates a coupling strength B that is sufficiently large to transmit the desired power P^d. Furthermore, a stable fixed point can only be found if the chosen reactive power droop gain χ does not exceed a critical value.

To understand the stability of droop-controlled inverters in extended networks, we examined the full set of equations of motion for arbitrary networks of inverters in a lossless setting. We decomposed the voltage and power-phase-angle dynamics and employed linear stability analysis, resulting in the central stability conditions summarized in Lemma 2. Using these results, we were able to formulate several explicit stability criteria (Corollaries 1 to 5). Therein, a set of stability conditions are given as a set of inequalities, involving the isolated frequency and voltage subsystems as well as the full system. Notably, connectivity bounds for the full system are tighter than for the isolated subsystems, as shown in Corollary 3. Furthermore, an upper bound for the reactive power droop gains χ is given in Corollary 4. Since the droop gains can be programmed and chosen freely for each inverter, uncovering the upper bounds for these droop gains is needed to guarantee a stable operating state is obtained.

Subsequently, we numerically tested the derived stability criteria for two test systems by comparing the stability given by the full Jacobian to the one predicted by the derived sufficient stability criteria. In general, Corollaries 4 and 5 capture the shape of the parameter regions with a stable fixed point well. The parameter region that is stable according to the full Jacobian is larger than the stable parameter region that is stable according to Corollaries 4 and 5. This discrepancy is larger for the larger test system network. While a general statement about the tightness of the corollaries requires further investigation of different network ensembles, which should also consider heterogeneous parameters, Corollaries 4 and 5 are sufficient conditions for the stability of the considered fixed point. Thus, it is to be expected that they underestimate the size of the stable parameter region and therefore represent a conservative estimate.

Finally, the analytical treatment of droop-controlled inverters can be used to understand the dynamics of power grids that are driven by an increasing share of inverter-connected generation by solar and wind resources. The insights obtained by the derived stability conditions can be used to test the parametric dependencies of the stability regions. In particular, the analytic results highlight the interplay of the internal parameters of the inverters, such as the reactive power droop gain χ, and network properties, such as the algebraic connectivity λ_2.

REFERENCES

[1] R. Sims, P. Mercado, W. Krewitt, G. Bhuyan, D. Flynn, H. Holttinen, G. Jannuzzi, S. Khennas, Y. Liu, and L. J. Nilsson, *Integration of Renewable Energy Into Present and Future Energy Systems*. Cambridge, U.K.: Cambridge Univ. Press, 2011, pp. 609–706.

[2] M. Anvari, G. Lohmann, M. Wächter, P. Milan, E. Lorenz, D. Heinemann, M. R. R. Tabar, and J. Peinke, "Short term fluctuations of wind and solar power systems," *New J. Phys.*, vol. 18, no. 6, Jun. 2016, Art. no. 063027.

[3] B. Schäfer, C. Beck, K. Aihara, D. Witthaut, and M. Timme, "Non-Gaussian power grid frequency fluctuations characterized by Lévy-stable laws and superstatistics," *Nature Energy*, vol. 3, no. 2, pp. 119–126, Jan. 2018.

[4] J. Weber, M. Reyers, C. Beck, M. Timme, J. G. Pinto, D. Witthaut, and B. Schäfer, "Wind power persistence characterized by superstatistics," *Sci. Rep.*, vol. 9, no. 1, p. 19971, Dec. 2019.
[5] T. Pesch, H.-J. Allelein, and J.-F. Hake, "Impacts of the transformation of the German energy system on the transmission grid," *Eur. Phys. J. Special Topics*, vol. 223, no. 12, pp. 2561–2575, Oct. 2014.
[6] J. A. P. Lopes, C. L. Moreira, and A. G. Madureira, "Defining control strategies for MicroGrids islanded operation," *IEEE Trans. Power Syst.*, vol. 21, no. 2, pp. 916–924, May 2006.
[7] J. Rocabert, A. Luna, F. Blaabjerg, and P. Rodríguez, "Control of power converters in AC microgrids," *IEEE Trans. Power Electron.*, vol. 27, no. 11, pp. 4734–4749, Nov. 2012.
[8] R. Teodorescu, M. Liserre, and P. Rodriguez, *Grid Converters for Photovoltaic and Wind Power Systems*. West Sussex, U.K.: Wiley, 2011.
[9] F. Milano, F. Dörfler, G. Hug, D. J. Hill, and G. Verbic, "Foundations and challenges of low-inertia systems (invited paper)," in *Proc. Power Syst. Comput. Conf. (PSCC)*, Jun. 2018, pp. 1–25.
[10] R. Henriquez-Auba, J. D. Lara, C. Roberts, and D. S. Callaway, "Grid forming inverter small signal stability: Examining role of line and voltage dynamics," in *Proc. IECON 46th Annu. Conf. IEEE Ind. Electron. Soc.*, Oct. 2020, pp. 4063–4068.
[11] R. Henriquez-Auba, J. Daniel Lara, and D. S. Callaway, "Small-signal stability of load and network dynamics on grid-forming inverters," 2022, *arXiv:2212.08147*.
[12] J. W. Simpson-Porco, F. Dörfler, and F. Bullo, "Synchronization and power sharing for droop-controlled inverters in islanded microgrids," *Automatica*, vol. 49, no. 9, pp. 2603–2611, Sep. 2013.
[13] J. Schiffer, D. Efimov, and R. Ortega, "Global synchronization analysis of droop-controlled microgrids—A multivariable cell structure approach," *Automatica*, vol. 109, Nov. 2019, Art. no. 108550.
[14] A. S. Matveev, J. E. Machado, R. Ortega, J. Schiffer, and A. Pyrkin, "A tool for analysis of existence of equilibria and voltage stability in power systems with constant power loads," *IEEE Trans. Autom. Control*, vol. 65, no. 11, pp. 4726–4740, Nov. 2020.
[15] H. Bai, H. Zhang, H. Cai, and J. Schiffer, "Voltage regulation and current sharing for multi-bus DC microgrids: A compromised design approach," *Automatica*, vol. 142, Aug. 2022, Art. no. 110340.
[16] P. Jaros, R. Levchenko, T. Kapitaniak, J. Kurths, and Y. Maistrenko, "Asymmetry induces critical desynchronization of power grids," *Chaos, Interdiscipl. J. Nonlinear Sci.*, vol. 33, no. 1, Jan. 2023, Art. no. 011104.
[17] F. Hellmann, P. Schultz, P. Jaros, R. Levchenko, T. Kapitaniak, J. Kurths, and Y. Maistrenko, "Network-induced multistability through lossy coupling and exotic solitary states," *Nature Commun.*, vol. 11, no. 1, p. 592, Jan. 2020.
[18] C. Balestra, F. Kaiser, D. Manik, and D. Witthaut, "Multistability in lossy power grids and oscillator networks," *Chaos, Interdiscipl. J. Nonlinear Sci.*, vol. 29, no. 12, Dec. 2019, Art. no. 123119.
[19] S. Tamrakar, M. Conrath, and S. Kettemann, "Propagation of disturbances in AC electricity grids," *Sci. Rep.*, vol. 8, no. 1, p. 6459, Apr. 2018.
[20] J. Schiffer, R. Ortega, A. Astolfi, J. Raisch, and T. Sezi, "Conditions for stability of droop-controlled inverter-based microgrids," *Automatica*, vol. 50, no. 10, pp. 2457–2469, Oct. 2014.
[21] J. Schiffer, T. Seel, J. Raisch, and T. Sezi, "Voltage stability and reactive power sharing in inverter-based microgrids with consensus-based distributed voltage control," *IEEE Trans. Control Syst. Technol.*, vol. 24, no. 1, pp. 96–109, Jan. 2016.
[22] P. C. Böttcher, D. Witthaut, and L. Rydin Gorjão, "Dynamic stability of electric power grids: Tracking the interplay of the network structure, transmission losses, and voltage dynamics," *Chaos, Interdiscipl. J. Nonlinear Sci.*, vol. 32, no. 5, May 2022, Art. no. 053117.
[23] J. Machowski, Z. Lubosny, J. W. Bialek, and J. R. Bumby, *Power System Dynamics: Stability and Control*, 3rd ed. New York, NY, USA: Wiley, 2020.
[24] E. A. A. Coelho, P. C. Cortizo, and P. F. D. Garcia, "Small-signal stability for parallel-connected inverters in stand-alone AC supply systems," *IEEE Trans. Ind. Appl.*, vol. 38, no. 2, pp. 533–542, 2002.
[25] F. Dorfler and F. Bullo, "Kron reduction of graphs with applications to electrical networks," *IEEE Trans. Circuits Syst. I, Reg. Papers*, vol. 60, no. 1, pp. 150–163, Jan. 2013.
[26] M. Newman, *Networks: An Introduction*, 2nd ed. Oxford, U.K.: Oxford Univ. Press, 2018.
[27] D. Manik, M. Timme, and D. Witthaut, "Cycle flows and multistability in oscillatory networks," *Chaos, Interdiscipl. J. Nonlinear Sci.*, vol. 27, no. 8, Aug. 2017, Art. no. 083123.
[28] S. H. Strogatz, *Nonlinear Dynamics and Chaos: With Applications to Physics, Biology, Chemistry, and Engineering*, 2nd ed. Boca Raton, FL, USA: CRC Press, 2015.
[29] P. Kundur, J. Paserba, V. Ajjarapu, G. Andersson, A. Bose, C. Canizares, N. Hatziargyriou, D. Hill, A. Stankovic, C. Taylor, T. V. Cutsem, and V. Vittal, "Definition and classification of power system stability IEEE/CIGRE joint task force on stability terms and definitions," *IEEE Trans. Power Syst.*, vol. 19, no. 3, pp. 1387–1401, May 2004.
[30] F. Zhang, *The Schur Complement and its Applications*, vol. 4, 1st ed. New York, NY, USA: Springer, 2005.
[31] W. Chen, D. Wang, J. Liu, T. Basar, K. H. Johansson, and L. Qiu, "On semidefiniteness of signed Laplacians with application to microgrids," *IFAC-PapersOnLine*, vol. 49, pp. 097–102, Jan. 2016.
[32] W. Chen, J. Liu, Y. Chen, S. Z. Khong, D. Wang, T. Basar, L. Qiu, and K. H. Johansson, "Characterizing the positive semidefiniteness of signed Laplacians via effective resistances," in *Proc. IEEE 55th Conf. Decis. Control (CDC)*, Dec. 2016, pp. 985–990.
[33] Y. Song, D. J. Hill, and T. Liu, "Small-disturbance angle stability analysis of microgrids: A graph theory viewpoint," in *Proc. IEEE Conf. Control Appl. (CCA)*, Sep. 2015, pp. 201–206.
[34] D. Zelazo and M. Bürger, "On the definiteness of the weighted Laplacian and its connection to effective resistance," in *Proc. 53rd IEEE Conf. Decis. Control*, Dec. 2014, pp. 2895–2900.
[35] M. Fiedler, "Algebraic connectivity of graphs," *Czechoslovak Math. J.*, vol. 23, no. 2, pp. 298–305, 1973.
[36] M. Fiedler, "A property of eigenvectors of nonnegative symmetric matrices and its application to graph theory," *Czechoslovak Math. J.*, vol. 25, no. 4, pp. 619–633, 1975.
[37] F. R. K. Chung and F. C. Graham, *Spectral Graph Theory*, 1st ed. Providence, RI, USA: American Mathematical Society, 1997.
[38] K. Sharafutdinov, L. Rydin Gorjão, M. Matthiae, T. Faulwasser, and D. Witthaut, "Rotor-angle versus voltage instability in the third-order model for synchronous generators," *Chaos, Interdiscipl. J. Nonlinear Sci.*, vol. 28, no. 3, Mar. 2018, Art. no. 033117.
[39] S. Geršgorin, "Über die abgrenzung der eigenwerte einer matrix," *Izvestiya Akademii Nauk SSSR, Otdelenie Matematicheskikh i Estestvennykh Nauk*, vol. 6, pp. 749–754, Jan. 1931. [Online]. Available: https://zbmath.org/?q=an:0003.00102|57.1340.0z

PHILIPP C. BÖTTCHER received the B.Sc. and M.Sc. degrees in physics from the University of Bremen, Germany. He was a Researcher with the DLR Institute of Networked Energy Systems, Oldenburg, Germany. He is currently a Researcher with the Institute of Energy and Climate Research, Forschungszentrum Jülich, Germany.

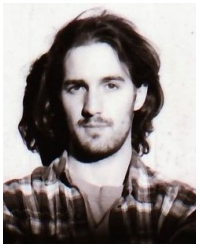

LEONARDO RYDIN GORJÃO received the B.Sc. degree in physics from the University of Lisbon, Portugal, the M.Sc. degree in physics from the University of Bonn, Germany, and the Ph.D. degree in physics from the University of Cologne, Germany. Currently, he is an Associate Professor with the Norwegian University of Life Sciences, Norway.

DIRK WITTHAUT received the Diploma and Ph.D. degrees in physics from the Technical University of Kaiserslautern, Germany, in 2004 and 2007, respectively. He was a Postdoctoral Researcher with the Niels Bohr Institute, Denmark, and the Max Planck Institute for Dynamics and Self-Organization, Germany. He was a Guest Lecturer with the Kigali Institute for Science and Technology, Rwanda. Since 2014, he has been leading a research group with the Forschungszentrum Jülich, Germany. He is currently a Full Professor with the University of Cologne, Germany.